Effect of Carbide Orientation on Wear Characteristics of High-Alloy Wear-Resistant Cast Irons

Yila Gaqi [1], Kenta Kusumoto [1,*], Kazumichi Shimizu [1] and Riki Hendra Purba [1,2]

[1] Graduate School of Engineering, Muroran Institute of Technology, 27-1 Mizumoto, Muroran City 050-8585, Japan

[2] Department of Mechanical Engineering, University of Sumatera Utara, Medan 20155, Indonesia

* Correspondence: kusumoto@mmm.muroran-it.ac.jp; Tel.: +81-143-46-5952; Fax: +81-143-46-5953

Abstract: Both erosive and abrasive wear are common in mechanical systems and moving components in industrial production. Once they occur in machine parts, the task of breakdown maintenance should be carried out, leading to high production costs. Previous research has shown that high-chromium cast iron (HCCI), a commonly used wear-resistant material, experiences repeated particle impacts that break up the chromium carbides (M_7C_3) on its surface, resulting in the formation of fine fracture carbides. It has been reported that erosion wear occurs progressively due to the shedding of protrusions caused by the plastic deformation of the material's matrix. Thus, the erosion wear characteristics of a material are strongly affected by carbides, which come in various shapes and can affect resistance. This research examined the orientation of carbides on the microstructure and their effects on erosion and abrasion properties. The wear tests showed that 27 wt.% chromium content high-alloy cast irons showed the best wear resistance properties due to the coarse strips of M_7C_3 carbides that effectively suppressed wear propagation. Additionally, the M_2C carbides crystallized around the M_7C_3 carbides which support the M_7C_3 carbide to reduce plastic deformation and carbide peel-out. Consequently, the wear resistance properties of this material are significantly improved.

Keywords: wear; carbide orientation; crack; plastic deformation

1. Introduction

The gradual removal of material from a surface as a result of contact and relative movement between two surfaces is called wear. The main types of wear are abrasive wear, adhesive wear, corrosive wear, erosion wear, micromotional wear, and cavitation wear. They depend on the specific mechanism involved and the equipment or material [1–4]. Of these, abrasive wear and erosion wear have significantly high rates of material removal compared to the other wear types. These two types of wear occur when hard particles or abrasives come into contact with a surface and cause the removal of material by scraping or plowing and when they are caused by the impact of solid particles or fluids on the surface, resulting in the removal of material. They occur mainly in sliding contact in crushers, gears, bearings, pistons, and valves and in pumps, valves, and nozzles in the mining, ironmaking, chemical, and petroleum industries [5–8].

The relatively high cost-effectiveness of HCCI compared to some other wear-resistant materials results in it being an excellent wear-resistant material, and it is widely used in many applications [6,9–19]. This is because HCCI typically exhibits a hardness of between 650 and 850 HV. Its high hardness makes it extremely resistant to either erosive or abrasive wear. Furthermore, the high hardness phase named the carbide and the presence of up to 30% carbide volume fraction (CVF) of chromium carbides (M_7C_3) dispersed in the microstructure of HCCI provides the material with exceptional wear resistance. These hard carbides act as a barrier to prevent direct contact between the material and the abrasive particles, thus reducing the wear rate to a minimum. Furthermore, it can be easily cast into

complex shapes and sizes, making it suitable for a wide range of components in industries such as mining, cement, power generation, and mineral processing. Many researchers have studied the effect of the small addition of transition metals to HCCI. For example, Touhami, R.C. [18] reported that the addition of trace (0–1 wt.%, hereafter as %) amounts of manganese (Mn) and niobium (Nb) can refine M_7C_3 carbides. However, the addition of a small amount (up to 3.47%) of Nb contributes to the hardness and wear resistance of the HCCI [14,15], and vanadium (V) [13] also has this effect. Furthermore, the addition of 2 wt.% titanium (Ti) can also refine the M_7C_3 carbide [17,19]. However, R. J. Chung et al. also reported that the M_7C_3 carbide was not refined at 6% Ti content. However, the wear of the HCCI is mainly due to the loss of wear resistance properties due to the fragmentation of the M_7C_3 carbide by plastic deformation and the impact or sliding of the particles. Therefore, adding one kind of element does not improve the wear resistance in terms of wear mechanism.

Hashimoto et al. [20] have developed a multi-component white cast iron (MWCI) for rolling rolls. The typical chemical composition of this material is Fe-2%C-5%Cr-5%V-5%Mo-5%W-Co. Plate-like M_2C carbides with a hexagonal lattice and petal-like MC carbides with a face-centered cubic lattice crystallize in the matrix upon solidification. Although the M_2C carbides reacted with austenite and transformed into MC, M_6C, and M_7C_3 carbides during heat treatment, the carbide morphology remained unchanged. Inthidech et al. [21] investigated the three-body abrasive wear behavior of several heat-treated multi-alloyed white cast irons. These multi-alloyed white cast irons contain from 1.73 to 2.34% C and 5% Cr, molybdenum (Mo), tungsten (W), V, and 2% cobalt (Co). According to the results, the carbides precipitated in the matrix are almost MC carbides and M_2C carbides. Furthermore, regardless of the automatizing temperature, the hardness is proportional to the retained austenite at volume fractions above 10%. Additionally, Kusumoto et al. [22] fabricated a new MWCI by adding strong carbide-forming elements such as Cr, Nb, Mo, W, and Co to white cast iron at around 5 wt.%. The experimental results show that although the CVF of MWCI is only about 20 wt.%, MWCI shows excellent wear resistance compared to 27 wt.% Cr addition HCCI (27Cr-WCI). The MWCIs named 5V-5Co and 5Nb-5Co showed the best wear resistance. Kusumoto reported that in addition to the higher hardness, this is most probably due to the precipitation of several types of high-hardness carbides during solidification, such as MC, M_2C (or M_6C), and M_7C_3 carbides.

Based on the wear characteristics of HCCI and MWCI described above, a new material with enhanced wear resistance, called high-chromium-based multi-component white cast iron (Hi-Cr-based MWCI), has been fabricated by Purba et al. [23]. It is produced by adding 3 wt.% of strong carbide-forming elements such as V, Mo, W, and Co to HCCI. Hi-Cr-based MWCI is reported to have a higher CVF than HCCI and a harder hardness than MWCI as well as several types of high-hardness carbides during solidification, such as M_7C_3 and M_2C carbides. It is important to note here that the matrix of these high-alloy wear-resistant cast irons exhibits high hardness martensite by means of the corresponding heat treatment.

It can be found that in addition to hardness and CVF, the orientation of the carbide plays a crucial role in the wear characteristics of these materials. However, its specific effect has not yet been discussed in detail. Therefore, in the present research, the effect of carbide orientation on the wear characteristics of several high-alloy wear-resistant cast irons was investigated by observing the wear characteristics in erosion wear tests and abrasive wear tests.

2. Materials and Methods

2.1. Materials

The chemical composition of the four high-alloy wear-resistant cast irons investigated in the present research is shown in Table 1. The irons consist of 27% Cr content white cast iron (27Cr-WCI), 5% V and 5% Co content MWCI (5V-MWCI), 5% Nb and 5% Co content MWCI (5Nb-MWCI), and 27% Cr content Hi-Cr-based MWCI (27Cr-MWCI), and 27Cr-WCI was used as comparison material. A high-frequency induction furnace was

used to manufacture these four kinds of irons. The pouring temperature of 27Cr-WCI and 27Cr-MWCI is 1823K, and the pouring temperature of 5V-MWCI and 5Nb-MWCI is 1853 K. A total of 50 kg of raw material of each specimen was converted to a molten state at 1973 K by means of an induction furnace and then poured into a Y-sand-block-mold. Then, the lower part ($53 \times 53 \times 125$ mm^3) of the Y-block was cut into a number of wear test specimens of $50 \times 50 \times 10$ mm^3. Finally, the surface of the specimen was ground to a roughness of approximately 0.2 µm Ra to standardize the initial conditions of the test surface.

Table 1. Chemical composition of specimens.

Material	C	Si	Mn	Cr	V	Nb	Mo	W	Co	Fe
27Cr-WCI	3.07	0.62	0.47	27.45	-	-	-	-	-	Bal.
5V-MWCI	1.97	0.69	0.27	4.57	5.23	-	5.36	5.34	4.30	Bal.
5Nb-MWCI	1.79	0.65	0.20	4.89	-	5.27	4.69	5.75	4.96	Bal.
27Cr-MWCI	2.9	0.46	0.39	27.50	2.95	-	2.85	2.92	2.98	Bal.

Considering the transformation of the austenitic matrix to martensite and the precipitation of secondary carbides, which is beneficial for strength and wear resistance [9], the materials were heat treated in this study. Based on the hardness shown after quenching in the range of 1173–1423 K and tempering in the range of 773–873 K, the materials were observed to show the highest hardness values at 1323 K for quenching and 798 K for tempering. Therefore, a heat treatment as shown in Figure 1 was used. The details are as follows: (1) quenching: kept at 1323 K for 3.6 ks followed by forced air cooling (F.A.C.) to room temperature and (2) tempering: kept at 798 K for 10.8 ks followed by air cooling (A.C.) to room temperature. It should be added that 27Cr-MWCI was not tempered in this study as the tempered 27Cr-MWCI showed lower wear resistance than the quenched 27Cr-MWCI in the previous study [23].
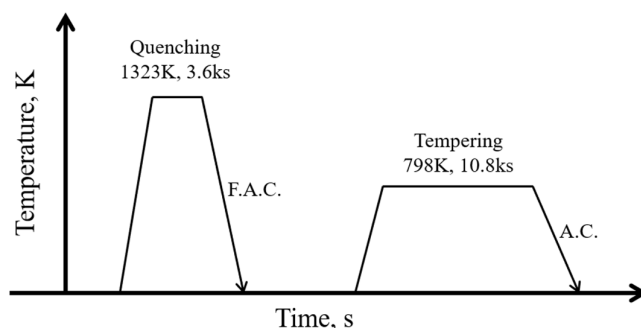

Figure 1. Heat treatment conditions.

An optical microscope (OM, ECLIPSE LV150N, Nikon, Minato, Japan) and two scanning electron microscopes (SEMs and EDS, JSM-6510A, JEOL, Akishima, Japan, and JXA-9800 R, Akishima, Japan) were used for observing the microstructure of each material. In addition, a VHX-1000 (KEYENCE, Japan) was used to measure the CVF of materials in the optical microscope images with a magnification of 100 times. A standard FV-800 Vickers hardness tester (FUTURE-TECH CORP., Kawasaki, Japan) was used to obtain the macro-hardness. The CVFs and Vickers hardness values are average values measured at 12 different positions. The samples were etched with 5% nital and used for microstructure analysis.

2.2. Methods

In this study, erosive wear and abrasive wear were carried out on the four high-alloy wear-resistant cast irons mentioned above to better understand the effect of carbide orientation on wear characteristics.

Figure 2a shows a schematic view of the suction-type blast machine and the steel grit being used as an impact particle used for the erosion wear test. Irregular steel grits

(2 kg) with a Vickers hardness of 810 HV and an average particle size of 770 μm were used and replaced after each test, considering that the size of the particles was changed by the erosion of the particles. The experimental conditions were an air velocity of approximately 100 m/s and a particle injection rate of 20 g/s. Impact angles α of 30, 60, and 90 deg. were used, and the duration of each test was 3600 s.
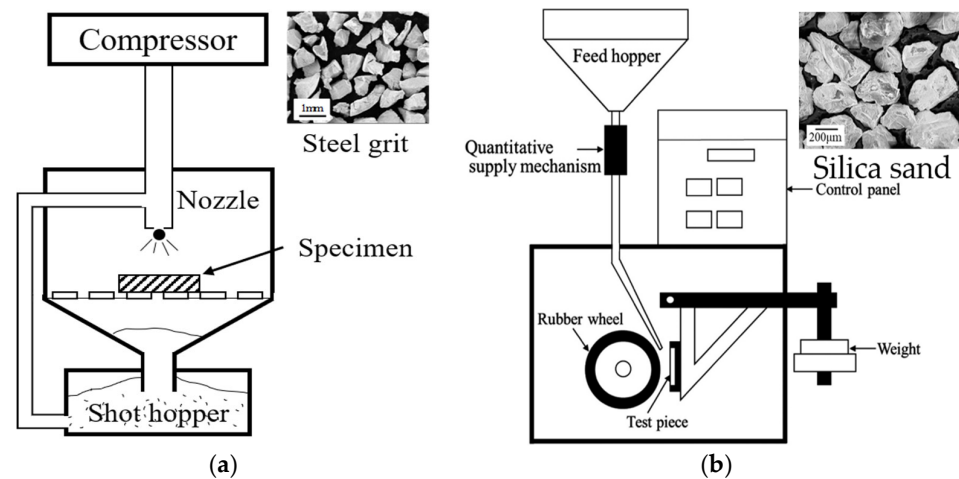

Figure 2. (**a**) Schematic view of suction-type blast machine and steel grit; (**b**) schematic view of the rubber-wheel abrasion tester and silica sand.

The schematic view of a rubber-wheel abrasion tester and the practical impact of silica sand No. 6 are shown in Figure 2b. The specimen was pressed against the circumference of a rubber wheel rotating at 100 rpm with a load of 196 N. Silica sand No. 6 (average grain size: 300 μm, hardness: 1100 HV) was fed at approximately 4.2 g/s during the test. The test duration was 360 s.

In both tests, the mass of the specimen was measured before and after the wear test using an electronic balance (measurement accuracy: 0.1 mg). For erosive wear, it is more accurate to compare material removed from specimens with different densities using volume loss rather than mass loss. The average density of the target material was used to calculate the erosion rate from the erosive volume. The erosion rate is defined as follows:

$$Erosion\ rate\left(cm^3/kg\right) = \frac{\left[mass\ removal\ per\ second(kg/s)/material\ density\left(kg/cm^3\right)\right]}{mass\ amount\ of\ impact\ particals\ per\ second(kg/s)} \tag{1}$$

The wear rate was used to evaluate the abrasive wear rate, which is obtained by dividing the amount of wear (Δm) by the distance used in this research. The formula is as follows:

$$Wearrate = \frac{\Delta m}{\pi dtn} \tag{2}$$

where d is the diameter of the rubber wheel, t is the test time, and n is the rotating speed.

3. Results

3.1. Microstructure

The microstructure observation, SEM, EDS results, macro hardness, and CVF of specimens are shown in Figure 3 (27Cr-WCI), Figure 4 (5V-MWCI), Figure 5 (5Nb-MWCI), and Figure 6 (27Cr-MCWI), respectively. The carbide precipitated by 27Cr-WCI is the M_7C_3 carbide and has a CVF of 32.6%. In the case of 5V-MWCI, it has a lower CVF of 18%, which is mainly M_2C and MC carbides. However, unlike 5V-MWCI, the MC carbide of 5Nb-MWCI is not only larger in grain size but also mostly precipitates as a population and has a different type of M_6C carbide. A small amount of M_7C_3 carbide, which is not easily observed on the optical microscope, was also observed in the EDS mapping results

of 5Nb-MWCI. Compared to the other three materials, 27Cr-MCWI showed a CVF of up to 34.9%, with the carbides being the M_7C_3 carbide, which is coarser than that of 27Cr-WCI, and a small amount of M_2C carbide. This is consistent with previous research findings that the M_7C_3 carbide precipitates as the predominant carbide type in the microstructure once the Cr addition is over 10% [12]. Moreover, no precipitation of the MC carbide was observed in 27Cr-MCWI. E. Cortés-Carrillo reported [16] that the MC carbide was not precipitated during solidification on the microstructure of HCCI with 2 wt.% V added. Moreover, the formula of secondary carbides on all specimens was determined as the $M_{23}C_6$ carbide through 10 repeated EDS point analyses of different carbides. Furthermore, the volume fraction of each carbide for four high-alloy wear-resistant cast irons is given in Table 2. Combining the volume fraction of each carbide with the SEM images, it can be seen that the M_7C_3 carbides of 27Cr-MWCI are coarser in size than those of 27Cr-WCI. as there is not much difference in their volume fraction. Additionally, the volume fraction of the secondary carbides of 27Cr-MWCI is lower compared to that of the other three materials, which can be attributed to the tempering treatment that was not experienced.
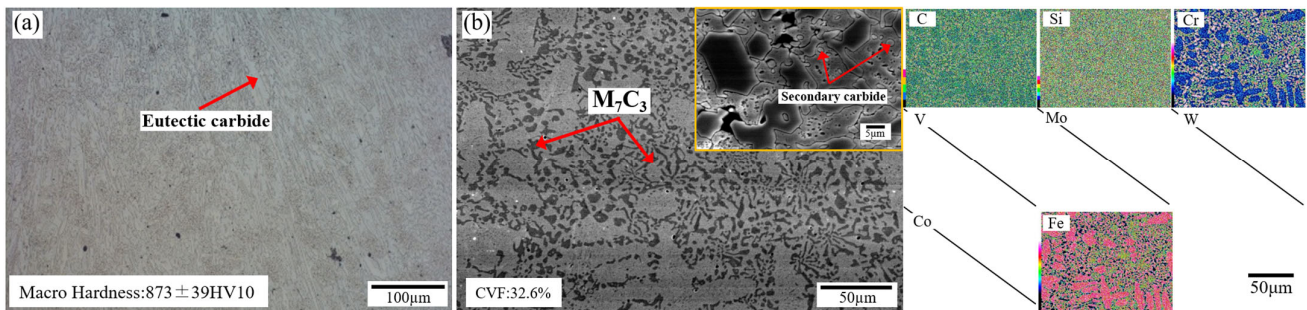

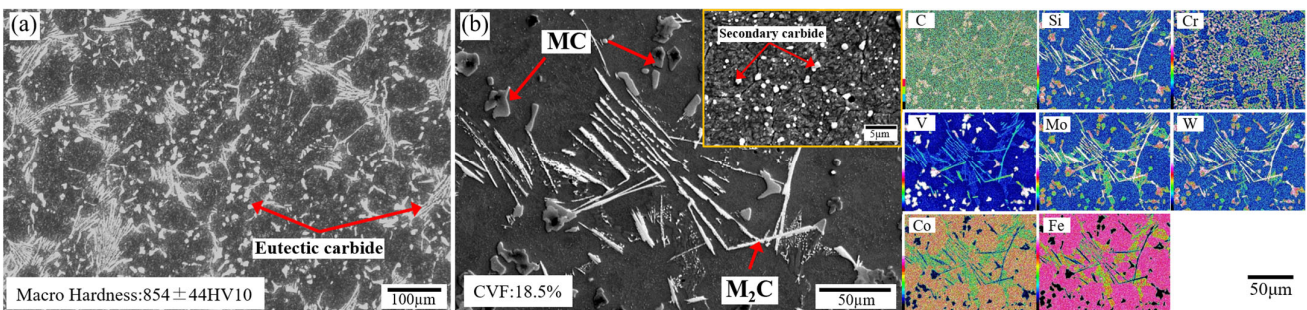**Figure 3.** SEM (**a**) and EDS (**b**) observation result of microstructure, hardness, and CVF of 27Cr-WCI.

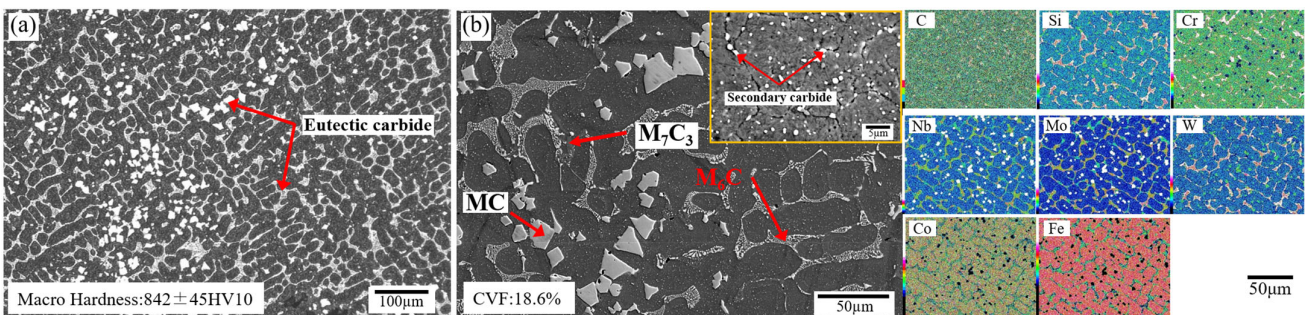**Figure 4.** SEM (**a**) and EDS (**b**) observation result of microstructure, hardness, and CVF of 5V-MWCI.

Figure 5. SEM (**a**) and EDS (**b**) observation result of microstructure, hardness, and CVF of 5Nb-MWCI.
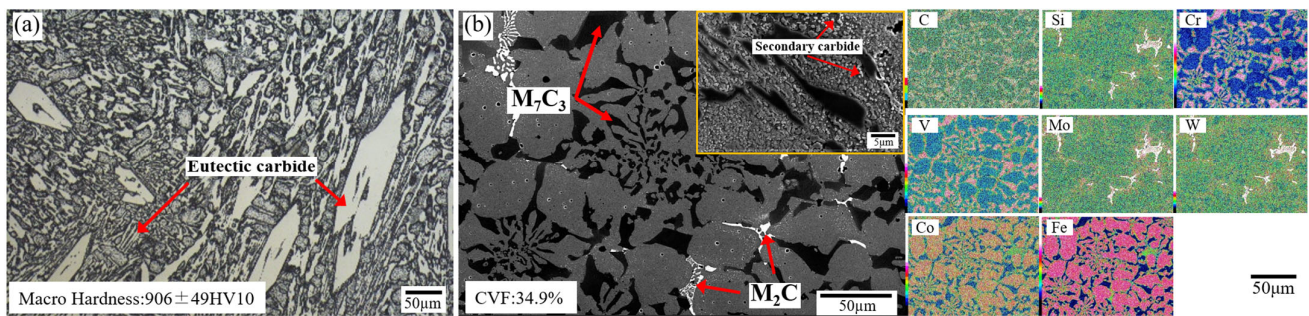
Figure 6. SEM (**a**) and EDS (**b**) observation result of microstructure, hardness, and CVF of 27Cr-MCWI.

Table 2. Each carbide volume fraction of specimens.

Material	MC	M_2C	M_6C	M_7C_3	$M_{23}C_6$
27Cr-WCI	-	-	-	29.3	3.3
5V-MWCI	7.4	6.0	-	-	5.1
5Nb-MWCI	5.3	-	5.9	3.8	3.6
27Cr-MCWI	-	2.3	-	30.5	2.1

Usually, the matrix of high-Cr white cast iron or multi-alloy cast iron changes from austenite form to martensite during the heat-treatment step. However, a small amount of retained austenite can still be found in the microstructure after heat treatment [21,22]. In the present study, the matrix of all studied materials shows that martensite is the majority matrix type, and the presence of retained austenite is hard to observe. The reason for the different results between this study and previous ones might be due to the difference in cooling rate, keeping time, and also overall chemical composition. The micro-Vickers hardness tester revealed that 27Cr-WCI showed a matrix hardness of 654 HV0.3, 5V-MWCI and 5Nb-MWCI had a matrix hardness of around 720 HV0.3, and 27Cr-MWCI had the highest matrix hardness at around 800 HV0.3. This should be related to the decrease in the C element content in the matrix due to the growth of secondary carbides during tempering treatment. Based on the results of macro-Vickers hardness tests at room temperature, 27Cr-WCI and 27Cr-MCWI show higher hardness than 5Nb-MWCI and 5V-MWCI due to the larger CVF and the large amount of the M_7C_3 carbide. The highest hardness of 27Cr-MCWI may be attributed to the coarser M_7C_3 carbide and harder matrix. Furthermore, as with the previous material [24], Co elements contributing to wear resistance were detected in the matrix.

3.2. Wear Characteristics

The results of the erosion and abrasive wear tests are given in Figure 7 with hardness. In the erosive wear test, 27Cr-MWCI showed the best wear resistance. In contrast, there was no significant difference in the erosion rate between the two MWCIs. As a comparison material, the erosion rate of 27Cr-MWCI was significantly higher than that of the other materials. Moreover, all materials showed the greatest angular dependence of the erosion rate at an impact angle of 60 deg.

In the abrasive wear test, it was also 27Cr-MWCI that showed the best wear resistance, while 5Nb-MWCI had slightly better wear resistance than 5V-MWCI. 27Cr-WCI also had the lowest wear resistance.

Overall, 27Cr-MWCI, the hardest material, showed the best wear resistance in both the erosion and abrasive wear tests. However, the second-hardest material, 27Cr-WCI, showed a higher erosion rate (and wear rates) than all materials, especially more than two times for 27-MWCI. These phenomena indicate that hardness is not the main factor affecting wear resistance. Additionally, an analysis of variance (ANOVA) was performed on the significance of the differences in wear rates between the different HACIs to determine whether the differences in wear resistance obtained from the tests were statistically significant. However,

considering the different wear mechanisms of erosion wear and abrasive wear, they were analyzed separately, and the results are given in Table 3. It should be mentioned that the erosion rate at an impact angle of 60 deg. was chosen for the investigation, since here the material erodes the fastest. ANOVA showed that both in erosion wear and abrasive wear, the sum of squares between (SSB) was greatly larger than the sum of squares within (SSW) and showed a significant variance ($p < 0.01$).
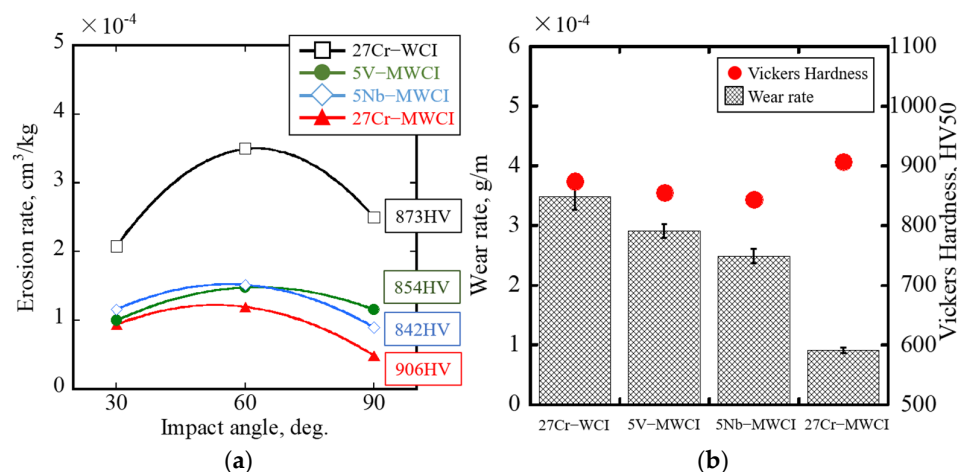

Figure 7. (**a**) Erosion rate of each material as a function of impact angle and hardness; (**b**) abrasive wear rate and hardness of each material.

Table 3. Results of ANOVA.

Test	Squares	Sum of Squares	df	Mean Square	F	$p\ (\propto < 0.05)$
Erosion (60 deg.)	Sum of Squares Between	10.105	3	3.368	137.199	<0.001
	Sum of Squares Within	0.196	8	0.025		
	Sum of Squares Total	10.301	11			
Abrasive	Sum of Squares Between	8.64	3	2.88	138.799	<0.001
	Sum of Squares Within	0.166	8	0.021		
	Sum of Squares Total	8.806	11			

4. Discussion

To clarify the correlation between wear resistance and CVF, the erosion and abrasive wear rates need to be compared with CVF. Here, considering the inconsistency in the units (evaluation method) of erosion and abrasive wear rates, the erosion and abrasive wear rates of 27Cr-WCI are defined as the denominator and the erosion and abrasive wear rates of other materials are defined as the numerator, and the wear rates were derived and plotted with the CVF and significance of each HACI in Figure 8. In terms of correlation, CVF does not seem to be the key to wear resistance either. This is because 27Cr-WCI has a CVF around 40% greater than that of 5V-MWCI and 5Nb-MWCI, but its wear rates are higher in erosion and abrasive wear tests.

In this regard, after deep etching the matrix of the materials with aqua regia, their precipitated carbides were observed by the SEM as given in Figure 9, which was used to investigate the effect of carbide orientation on wear characteristics. As seen from the depth etching results, the M_7C_3 carbide of 27Cr-WCI precipitates in long-isolated states, such as strip shape, rod shape, and hexagonal shape, in a single direction. As for 5V-MWCI, the M_2C carbide precipitates as a Christmas tree-like shape. Additionally, it is difficult to observe MC carbides on low-magnification deep etching SEM images, but some MC carbides can be observed on high-magnification lighter etching SEM images. These suggest

that the Christmas-tree-like M_2C of 5V-MWCI is distributed in the matrix in a stereoscopic direction, whereas the MC carbide is an isolated state present in the matrix and falls off once the matrix has been etched to a certain extent. Unlike 5V-MWCI, the M_6C carbide of 5Nb-MWCI is fishbone-like and thicker. In addition, the MC carbide is ortho-octahedral and is also not easily observed on deep etch SEM images. However, as with 5V-MWCI, the fishbone-like M_6C carbide of 5Nb-MWCI is distributed in the substrate in a stereoscopic direction, whereas the MC carbide groups are in an isolated state present in the matrix and falls off once the matrix is etched to a certain extent. The M_7C_3 carbide of 27Cr-MCWI precipitates like the M_7C_3 carbide of 27Cr-WCI but is much thicker. The fishbone-like M_2C carbide is observed distributed between the M_7C_3 carbide and/or bridging isolated states of the M_7C_3 carbide. Additionally, the composition of these carbides was measured using the point analysis function of EDS, and the results are shown in Table 4. It can be seen that V is involved in the precipitation of the MC carbides of MWCI and the M_7C_3 carbides of 27Cr-MWCI, respectively. The M_2C carbide is composed of Mo and/or W, which is consistent with the results found in the research of Xu L. [5]. Overall, each material shows its own carbide orientation as the shape and size of the precipitated carbides are strongly influenced by the overall chemical composition of the material. Therefore, an attempt is made next to discuss the effect of carbide orientation on the wear mechanism, starting with the observation of the wear state.
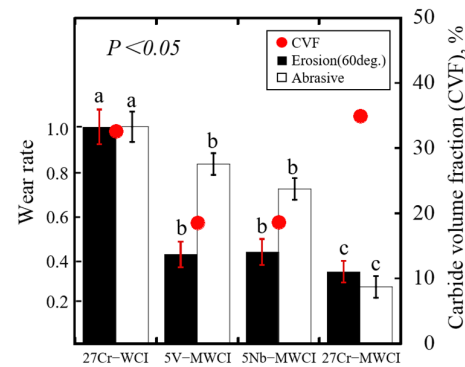

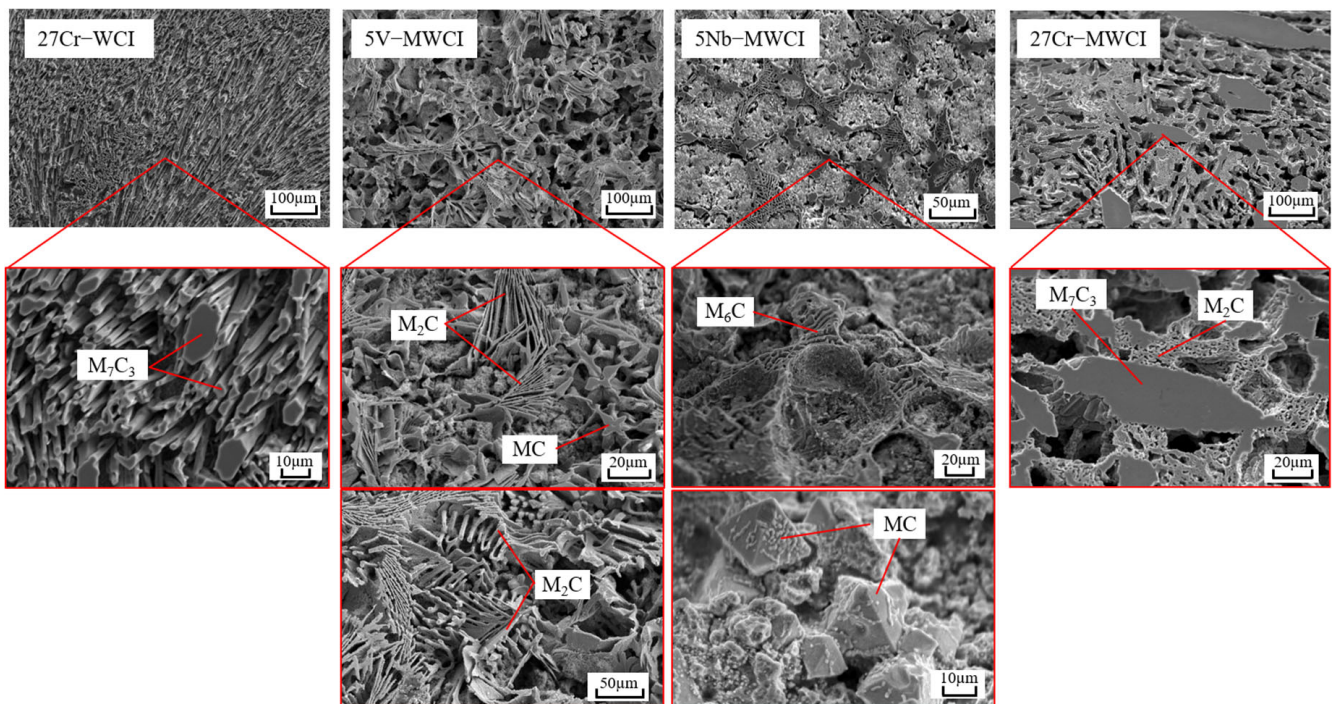**Figure 8.** Correlation between wear rate, significance, and CVF of each HACI.

Figure 9. Carbides orientation of materials after deep etching.

Table 4. Carbide type of specimens.

Material	MC	M$_2$C	M$_6$C	M$_7$C$_3$
27Cr-WCI	-	-	-	Cr$_7$C$_3$
5V-MWCI	VC	(Mo or W)$_2$C	-	-
5Nb-MWCI	NbC	-	(Fe,Mo or W)$_6$C	Cr$_7$C$_3$
27Cr-MCWI	-	(Mo,W)$_2$C	-	(Cr,V)$_7$C$_3$

Figure 10 shows the wear-surface SEM images of the materials. It can be observed that, as reported by K.-H. Zum Gahr [2], the wear of erosion abrasion comes mainly from the micro-cutting of the impacting particles, while that of abrasive wear is due to the micro-plowing of the particles.
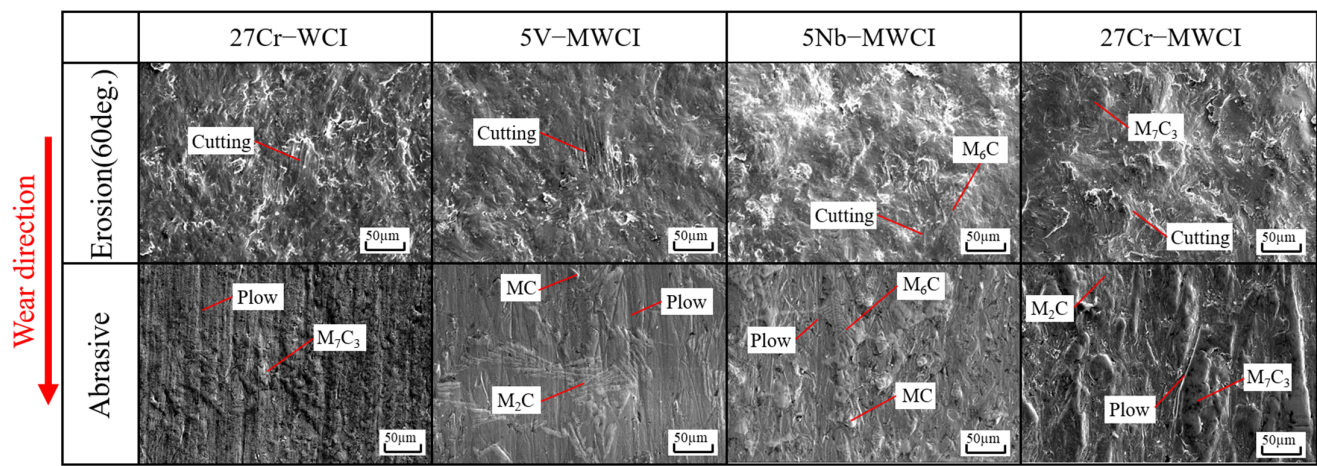
Figure 10. Wear-surface SEM images of the materials.

Different from the indistinctness of the erosion wear surfaces, the carbide wear state on the friction wear surfaces is more clearly defined. Some plow scars can be observed on the surface of each material but with some variation. The plow scars on 27Cr-WCI are deep and straight, indicating that the micro-plowing of the particles was smooth and not significantly hindered. On the other hand, deeper plow scars on the matrix and shallow and shorter plow scars on the carbide can be observed on the surfaces of the other materials, particularly 5Nb-MWCI and 27Cr-MCWI. This indicates that the micro-plowing of the particles is being obstructed from the carbides. For a clearer understanding, the wear cross-sections of 5Nb-MWCI and 27Cr-MCWI were observed, and then a mechanistic representation was drawn as shown in Figure 11.

With regard to 5Nb-MWCI, due to the high hardness and uniform distribution of the M$_6$C carbide throughout the matrix, the particles cannot plow the M$_6$C carbide as well as the relatively soft matrix, leaving only shallow plow marks. The MC carbide can also act as a barrier to micro-plowing, but due to its small size and high isolation, it tends to fall off when the surrounding matrix is worn. However, when the surrounding matrix is worn to a certain depth, the M$_6$C carbide cracks. Then, as the M$_6$C carbide falls off as a whole, the MC carbide behind it falls off with it.

It is well known that the wear of 27Cr-WCI is mainly due to the cracking of the M$_7$C$_3$ carbide as a result of plastic deformation of the wear surface. This is not the case with 27Cr-MCWI. Due to the anchor effect of the M$_2$C carbide precipitated around the M$_7$C$_3$ and the coarser M$_7$C$_3$ carbide, not only is the plastic deformation suppressed, but also the wear of the matrix becomes shorter and shallower, even though the M$_7$C$_3$ carbides are bracken by the particles. This is because if there is no surrounding precipitation of the M$_2$C carbide, the finer M$_7$C$_3$ carbide still cracks due to the plastic deformation of the matrix, and the crack of the coarser M$_7$C$_3$ carbide is deeper than that of the finer M$_7$C$_3$ carbide. Therefore, it can be said that the precipitation of 2.3% CVF of the fishbone-like M$_2$C carbide

played a positive role in the wear resistance, resulting in 27Cr-MCWI showing the best wear resistance in this work. Furthermore, it may be a good future research direction to precipitate a more uniform fishbone-like M_2C carbide in the MCWI.
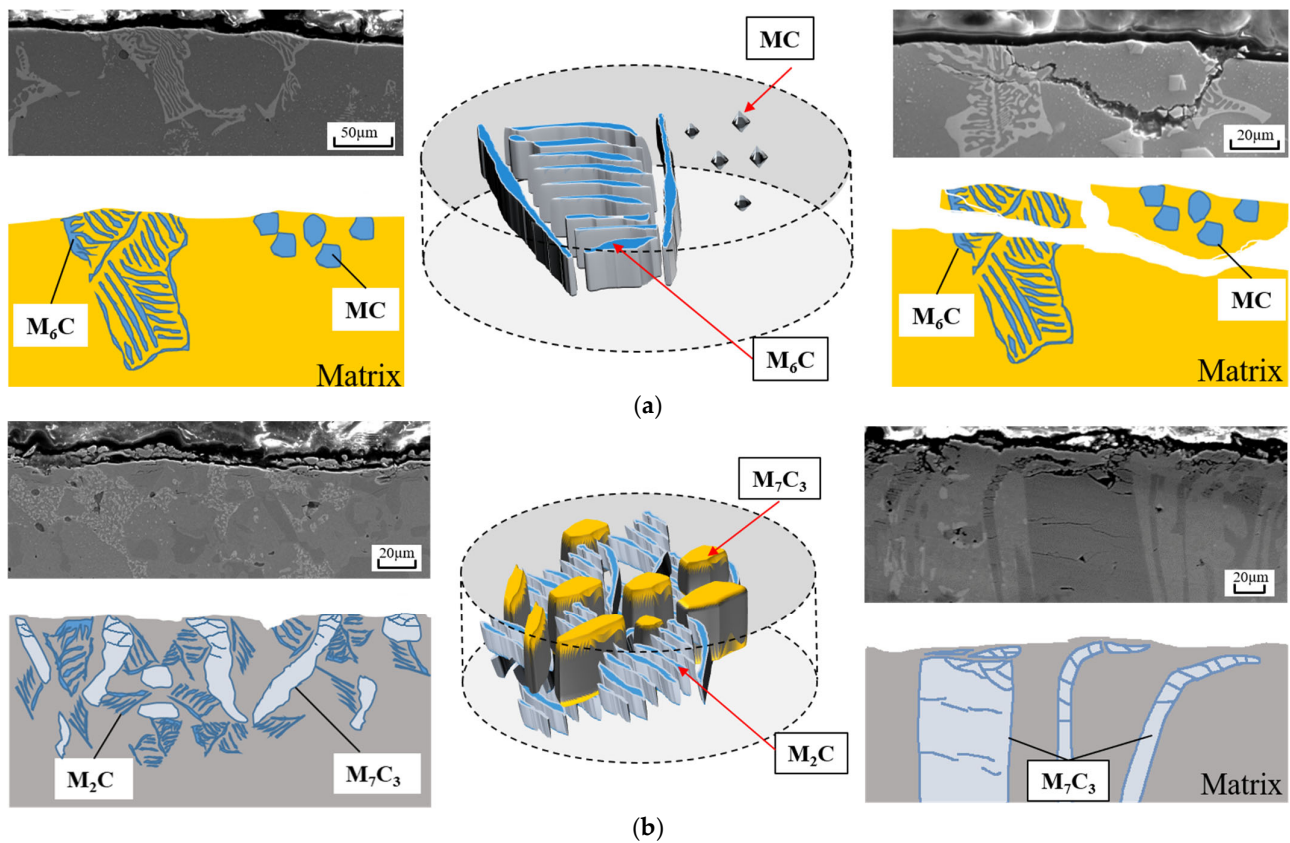

Figure 11. Schematic of wear mechanism via cross-section of (**a**) 5Nb-MWCI and (**b**) 27Cr-MCWI.

It is worth noting that the role of secondary carbides was not observed in the results of the wear condition and wear mechanism observations. This is probably due to the fact that the effect of secondary carbides is not reflected in the wear mechanism but in the strengthening of the matrix.

5. Conclusions

In the present research, the effect of carbide orientation on the wear characteristics of several high-alloy wear-resistant cast irons was investigated by observing the wear characteristics in erosion wear tests and abrasive wear tests. All results and discussions can be summarized in the following points.

1. The M_7C_3 carbide of 27Cr-WCI precipitates in long-isolated states, such as strip shape in a single direction.
2. The M_2C carbide is Christmas-tree-like in 5V-MWCI and fishbone-like in 5Nb-MWCI and 27Cr-MCWI. The M_6C carbide is fishbone-like in 5Nb-MWCI, and the MC carbides are isolated grains in 5V-MWCI, grouped octahedral grains in 5Nb-MWCI, and are not precipitated in 27Cr-MCWI.
3. 27Cr-MCWI shows the best wear resistance due to its coarse M_7C_3 carbide and the anchoring effect of the fishbone-like M_2C carbide distributed around the M_7C_3 carbide, which inhibits plastic deformation and reduces the amount of matrix being worn.

Conflicts of Interest: The authors declare no conflict of interest.

References

1. Finnie, I. Erosion of surface by solid particles. *Wear* **1960**, *3*, 87–103. [CrossRef]
2. Gahr, K.-H.Z. Wear by hard particles. *Tribol. Int.* **1998**, *31*, 587–596. [CrossRef]
3. Kenneth, H.; Erdemir, A. Influence of tribology on global energy consumption, cost and emissions. *Friction* **2017**, *5*, 263–284.
4. Xu, L.; Wang, F.; Li, M.; Li, F.J.; Wang, X.D.; Jiang, T.; Deng, X.T.; Wei, S.Z. Fabrication and abrasive wear property of high chromium cast iron with high vanadium and high nitrogen content (HCCI-VN). *Wear* **2023**, *523*, 204828. [CrossRef]
5. Gussmagg, J.; Pusterhofer, M.; Summer, F.; Grün, F. Experimental visualization of the wear and scuffing evolution of a flake graphite cast iron cylinder liner. *Wear* **2023**, *526*, 204948. [CrossRef]
6. Wang, S.; Li, Y.; Wang, J.; Luo, T.; Zheng, Z.; Long, J.; Zheng, K.; Zhang, J. Effect of in-situ (Ti&W) C multiphase particles on three-body abrasive wear of high chromium cast iron. *Mater. Chem. Phys.* **2023**, *295*, 127161.
7. Wang, Y.; Fan, L.; Chen, H. Effect of strength and toughness of ceramic particles on impact abrasive wear resistance of iron matrix composites. *Mater. Today Commun.* **2023**, *35*, 105689. [CrossRef]
8. de Melloa, J.D.B.; Polycarpoub, A.A. Abrasive wear mechanisms of multi-components ferrous alloys abraded by soft, fine abrasive particles. *Wear* **2010**, *269*, 911–920. [CrossRef]
9. Kishore, K.; Kumar, U.; Nanda, D.; Adhikary, M. Effect of soaking temperature on carbide precipitation, hardness, and wear resistance of high-chromium white cast iron. *J. Fail. Anal. Prev. Vol.* **2020**, *20*, 249–260. [CrossRef]
10. Tabrett, C.P.; Sare, I.R.; Ghomashchi, M.R. Microstructure-property relationships in high chromium white iron alloys. *Int. Mater. Rev.* **1996**, *41*, 59–82. [CrossRef]
11. Cetinkaya, C. An investigation of the wear behaviours of white cast Irons under different compositions. *Mater. Des.* **2006**, *27*, 437–445. [CrossRef]
12. Shimizu, K.; Purba, R.H.; Kusumoto, K.; Yaer, X.B.; Ito, J.; Kasuga, H.; Gaqi, Y.L. Microstructural evaluation and high-temperature erosion characteristics of high chromium cast irons. *Wear* **2019**, *426–427*, 420–427. [CrossRef]
13. Wang, H.; Yu, S.F.; Khan, A.R.; Huang, A.G. Effects of Vanadium on Microstructure and Wear Resistance of High Chromium Cast Iron Hardfacing Layer by Electroslag Surfacing. *Metals* **2018**, *8*, 458. [CrossRef]
14. Chen, H.X.; Chang, Z.C.; Lu, J.C.; Lin, H.T. Effect of niobium on wear resistance of 15%Cr white cast iron. *Wear* **1993**, *166*, 197–201.
15. Filipovic, M.; Kamberovic, Z.; Korac, M.; Gavrilovski, M. Microstructure and mechanical properties of Fe–Cr–C–Nb white cast irons. *Mater. Des.* **2013**, *47*, 41–48. [CrossRef]
16. Cortés-Carrillo, E.; Bedolla-Jacuinde, A.; Mejía, I.; Zepeda, C.M.; Zuno-Silva, J.; Guerra-Lopez, F.V. Effects of tungsten on the microstructure and on the abrasive wear behavior of a high-chromium white iron. *Wear* **2017**, *376–377*, 77–85. [CrossRef]
17. Chung, R.J.; Tang, X.; Li, D.Y.; Hinckley, B.; Dolman, K. Effects of titanium addition on microstructure and wear resistance of hypereutectic high chromium cast iron Fe–25wt.%Cr–4wt.%C. *Wear* **2009**, *267*, 356–361. [CrossRef]
18. Touhami, R.C.; Mechachti, S.; Bouhamla, K.; Hadji, A.; Khettache, A. Wear Behavior and Microstructure Changes of a High Chromium Cast Iron: The Combined Effect of Heat Treatment and Alloying Elements. *Metallogr. Microstruct. Anal.* **2023**, *37*, 1–11. [CrossRef]
19. Huq, M.J.; Shimizu, K.; Kusumoto, K.; Purba, R.H. Three-Body Abrasive Wear Performance of High Chromium White Cast Iron with Different Ti and C Content. *Lubricants* **2022**, *10*, 348. [CrossRef]
20. Hashimoto, M.; Kubo, O.; Matsubara, Y. Analysis of carbides in multi-component white cast iron for hot rolling mill rolls. *ISIJ Int.* **2004**, *44*, 372–380. [CrossRef]
21. Inthidech, S.; Opapaiboon, J.; Yamamoto, K.; Matsubara, Y. Three-Body-Type Abrasive Wear Behavior of Multi-Alloyed White Cast Iron with Different Carbon Contents Used for Hot Work Rolls. *ISIJ Int.* **2021**, *61*, 2832–2843. [CrossRef]
22. Kusumoto, K.; Shimizu, K.; Yaer, X.B.; Zhang, Y.; Ota, Y.; Ito, J. Abrasive wear characteristics of Fe-2C-5Cr-5Mo-5W-5Nb multi-component white cast iron. *Wear* **2017**, *376–377*, 22–29. [CrossRef]
23. Purba, R.H.; Shimizu, K.; Kusumoto, K.; Todaka, T.; Shirai, M.; Hara, H.; Ito, J. Erosive wear characteristics of high-chromium based multi-component white cast irons. *Tribol. Int.* **2021**, *159*, 106982. [CrossRef]
24. Kusumoto, K.; Shimizu, K.; Yaer, X.B.; Hara, H.; Tamura, K.; Kawai, H. High erosion-oxidation performance of Fe-based Nb or V containing multi-component alloys with Co addition at 1173 K. *Mater. Des.* **2015**, *88*, 366–374. [CrossRef]